

## Assembly of Core–Shell Structures for Photocatalytic Hydrogen Evolution from Aqueous Methanol

Han Zhou,<sup>†</sup> Erwin M. Sabio,<sup>‡</sup> Troy K. Townsend,<sup>‡</sup> Tongxiang Fan,<sup>†</sup> Di Zhang,<sup>†</sup> and Frank E. Osterloh<sup>\*‡</sup>

<sup>†</sup>State Key Laboratory of Metal Matrix Composites, Shanghai Jiaotong University, 800 Dongchuan Road, Shanghai, 200240, China, and <sup>‡</sup>Department of Chemistry, University of California, One Shields Avenue, Davis, California 95616

Received December 23, 2009. Revised Manuscript Received April 15, 2010

We present a layer-by-layer assembly approach for the construction of core–shell structures with photocatalytic activity for hydrogen evolution from aqueous methanol. Submicrometer silica spheres and ultrasonicated (TBA, H)Ca<sub>2</sub>Nb<sub>3</sub>O<sub>10</sub> and PA<sub>2</sub>K<sub>2</sub>Nb<sub>6</sub>O<sub>17</sub> nanosheets are used as the building blocks to assemble core–shell structures with single and double (homostacked and heterostacked) nanosheet layers via sequential electrostatic coupling with poly(diallyldimethylammonium) chloride (PDDA). The lateral nanosheet distribution on the SiO<sub>2</sub> spheres is observed with SEM while the stacking is directly observed with TEM. Diffuse reflectance UV/vis spectra reveal the nanosheet absorbance edge at ~350 nm. All core–shell structures are active for photocatalytic H<sub>2</sub> evolution from aqueous methanol solution with gas evolution rates comparable or smaller than observed for individually dispersed nanosheets. Heterostacks were more active than homostacks, with the latter being comparable to single layers (at equal mass). Loading with Pt nanoparticles increases H<sub>2</sub> evolution rates, but reduces the activity differences between homostacked and heterostacked samples.

### Introduction

Photocatalytic water splitting is a promising process to obtain hydrogen from renewable energy.<sup>1</sup> Many semiconductors catalyze the overall water splitting reaction, or one of the two half reactions.<sup>2</sup> Nanomaterials are particularly promising for these applications. Because of their small size, excitons and charges can reach the nanocrystal surfaces more easily,<sup>3,4</sup> and the large specific surface area of nanocrystals promotes reactions with substrates. For metal chalcogenides nanocrystals, quantum size confinement effects can be exploited to adjust the optical band gap, increasing the thermodynamic driving force for the coupled redox reactions. For CdSe nanoribbons, a quantum size effect establishes photocatalytic activity for the hydrogen evolution reaction, a reaction not catalyzed by bulk CdSe.<sup>5</sup> We recently showed that individually dispersed niobate and titanate nanosheets are catalysts for the photochemical H<sub>2</sub> evolution from sacrificial electron donors, and in the case of Pt-modified

HCa<sub>2</sub>Nb<sub>3</sub>O<sub>10</sub> nanosheets, water splitting into H<sub>2</sub> and peroxides.<sup>6–10</sup> These nanosheets are crystalline fragments of layered metal oxides with high photocatalytic activity for H<sub>2</sub> evolution from water and sacrificial donors.<sup>11–19</sup> The nanosheets are obtained by chemical exfoliation after exchanging the interlayer cations with soluble organic cations.<sup>20,21</sup> Because of their well-defined structural and

\*Corresponding author. Fax: (+1) 530 752 8995. Tel: (+1) 530 754 6242. E-mail: fosterloh@ucdavis.edu.

- (1) Kudo, A.; Miseki, Y. *Chem. Soc. Rev.* **2009**, 38(1), 253–278.
- (2) Osterloh, F. E. *Chem. Mater.* **2008**, 20(1), 35–54.
- (3) Kay, A.; Cesar, I.; Gratzel, M. *J. Am. Chem. Soc.* **2006**, 128(49), 15714–15721.
- (4) Law, M.; Greene, L. E.; Johnson, J. C.; Saykally, R.; Yang, P. D. *Nat. Mater.* **2005**, 4(6), 455–459.
- (5) Frame, F. A.; Carroll, E. C.; Larsen, D. S.; Sarahan, M. S.; Browning, N. D.; Osterloh, F. E. *Chem. Commun.* **2008**, 2206–2208.
- (6) Sarahan, M. C.; Carroll, E. C.; Allen, M.; Larsen, D. S.; Browning, N. D.; Osterloh, F. E. *J. Solid State Chem.* **2008**, 181(7), 1681–1686.

- (7) Compton, O. C.; Carroll, E. C.; Kim, J. Y.; Larsen, D. S.; Osterloh, F. E. *J. Phys. Chem. C* **2007**, 111(40), 14589–14592.
- (8) Compton, O. C.; Osterloh, F. E. *J. Phys. Chem. C* **2009**, 113(1), 479–485.
- (9) Compton, O. C.; Mullet, C. H.; Chiang, S.; Osterloh, F. E. *J. Phys. Chem. C* **2008**, 112(15), 6202–6208.
- (10) Allen, M. R.; Thibert, A.; Sabio, E. M.; Browning, N. D.; Larsen, D. S.; Osterloh, F. E. *Chem. Mater.* **2010**, 22(3), 1220–1228.
- (11) Maeda, K.; Mallouk, T. E. *J. Mater. Chem.* **2009**, 19(27), 4813–4818.
- (12) Maeda, K.; Eguchi, M.; Youngblood, W. J.; Mallouk, T. E. *Chem. Mater.* **2009**, 21(15), 3611–3617.
- (13) Miseki, Y.; Kato, H.; Kudo, A. *Energy. Environ. Sci.* **2009**, 2(3), 306–314.
- (14) Matsumoto, Y.; Koinuma, M.; Iwanaga, Y.; Sato, T.; Ida, S. *J. Am. Chem. Soc.* **2009**, 131(19), 6644–6645.
- (15) Ebina, Y.; Sakai, N.; Sasaki, T. *J. Phys. Chem. B* **2005**, 109(36), 17212–17216.
- (16) Ebina, Y.; Sasaki, T.; Harada, M.; Watanabe, M. *Chem. Mater.* **2002**, 14(10), 4390–4395.
- (17) Abe, R.; Shinohara, K.; Tanaka, A.; Hara, M.; Kondo, J. N.; Domen, K. *Chem. Mater.* **1997**, 9(10), 2179–2184.
- (18) Domen, K.; Kudo, A.; Shibata, M.; Tanaka, A.; Maruya, K.; Onishi, T. *J. Chem. Soc. Chem. Commun.* **1986**, No. 23, 1706–1707.
- (19) Domen, K.; Yoshimura, J.; Sekine, T.; Tanaka, A.; Onishi, T. *Catal. Lett.* **1990**, 4(4–6), 339–343.
- (20) Miyamoto, N.; Yamamoto, H.; Kaito, R.; Kuroda, K. *Chem. Commun.* **2002**, No. 20, 2378–2379.
- (21) Treacy, M. M. J.; Rice, S. B.; Jacobson, A. J.; Lewandowski, J. T. *Chem. Mater.* **1990**, 2(3), 279–286.

favorable physical properties, nanosheets are attractive building blocks for complex nanostructures with photocatalytic, optical and energy storage functions.<sup>22–34</sup> Nanosheet assemblies for solar energy conversion applications were pioneered in the laboratory of Tom Mallouk at PennState.<sup>35–38</sup> Here we show for the first time that layer-by-layer assembly of (TBA,H)Ca<sub>2</sub>Nb<sub>3</sub>O<sub>10</sub> and (PA)<sub>2</sub>K<sub>2</sub>Nb<sub>6</sub>O<sub>17</sub> nanosheets (PA = propylammonium; TBA = tetrabutylammonium) on silica microparticles generates core–shell type nanostructures that are active photocatalysts for H<sub>2</sub> evolution from aqueous solutions of methanol as sacrificial donor. Compared to the separate nanosheets, mixed nanosheet stacks exhibit mildly enhanced activity, suggesting the possibility of intersheet charge transfer. In addition to the photocatalytic properties we report the detailed assembly, TEM, UV/vis, and IR spectroscopic characterization of these materials. The presented method also provides a new pathway for the immobilization of photocatalysts on dispersible substrates. Such supported photocatalysts are more stable against aggregation under reactive conditions and can be easily recovered via sedimentation or filtration. This could be significant for photocatalytic water purification and for water splitting photocatalysis.<sup>39,40</sup>

### Experimental Section

**Materials.** K<sub>2</sub>CO<sub>3</sub> (98.5% purity), CaCO<sub>3</sub> (98.5%), Nb<sub>2</sub>O<sub>5</sub> (99.9% purity), propylamine hydrochloride (99+% purity),

propylamine, and TBA hydroxide (40 wt % in water) were obtained from Acros Organics. Hydrofluoric acid (49 wt % in water), poly(diallyldimethylammonium chloride) (PDDA, MW 10–20 × 10<sup>4</sup> g mol<sup>-1</sup>), tetraethylorthosilicate (TEOS) were received from Fisher Scientific. Hexachloroplatinic acid (H<sub>2</sub>PtCl<sub>6</sub>·6H<sub>2</sub>O) was obtained from Alfa Aesar. Water was purified by a Nanopure II system to a resistivity of > 18 MΩ cm. A Fisher Scientific Marathon 21000 centrifuge was employed for centrifugation. For ultrasonication, a Sonics Vibra Cell Ultrasonic Processor Model VCX130 was used in combination with a TI-6AL-4 V titanium alloy probe. The maximum power output is 130 W at a frequency of 20 kHz.

**Synthesis of Silica Spheres.** Four-hundred-fifty nanometer silica spheres were prepared according to a modified Stober method.<sup>41,42</sup> In a typical procedure, 12.0 mL of concentrated ammonium hydroxide was diluted to 100 mL with ethanol. To that was quickly added 3.5 mL (3.3 g, 16 mmol) of tetraethylorthosilicate under rapid stirring. The solution was left to stir for 8 h and slowly turned turbid white without observable precipitation. The resulting 450 nm SiO<sub>2</sub> spheres were centrifuged out of the dispersion at 8000 rpm and washed with ethanol four times, and then with deionized (DI) water three times. The product was redispersed in 250 mL of DI water and left to stir in an open flask at 60 °C to evaporate ammonium hydroxide until the pH of the solution was about 7.

**Synthesis of Nanosheets.** Colloidal suspensions of exfoliated PA<sub>2</sub>K<sub>2</sub>Nb<sub>6</sub>O<sub>17</sub> and TBA<sub>1-x</sub>H<sub>x</sub>Ca<sub>2</sub>Nb<sub>3</sub>O<sub>10</sub> nanosheets were synthesized according to reported procedures.<sup>6,43,44</sup> The resulting negatively charged nanosheets have a crystallographic thickness of 1–2 nm and a lateral size of several hundred nanometers as demonstrated in our previous study.<sup>6,7</sup> The as-obtained PA<sub>2</sub>K<sub>2</sub>Nb<sub>6</sub>O<sub>17</sub> nanosheets were ultrasonicated for 2 h to obtain small nanosheets for assembly while TBA<sub>1-x</sub>H<sub>x</sub>Ca<sub>2</sub>Nb<sub>3</sub>O<sub>10</sub> nanosheets were sonicated 50 min. The final pH of the nanosheets suspensions was 9–10. The sonicated nanosheets were then centrifuged (4200 rpm, 4 min) for purification to remove large-sized sheets and insoluble matter.

**Homostacked Assemblies.** A typical procedure for the Layer-by-layer (LBL) assembly of PDDA and TBA<sub>1-x</sub>H<sub>x</sub>Ca<sub>2</sub>Nb<sub>3</sub>O<sub>10</sub> nanosheets to form SiO<sub>2</sub>/(PDDA/TBA<sub>1-x</sub>H<sub>x</sub>Ca<sub>2</sub>Nb<sub>3</sub>O<sub>10</sub>)<sub>n</sub> (n = 1, 2) was conducted as follows: silica spheres (1.5 g) were ultrasonically dispersed in 150 mL of DI H<sub>2</sub>O containing 0.5 g of PDDA. The pH was adjusted to 9 by adding an appropriate amount of diluted TBAOH solution. The suspension was then stirred for 20 min to precoat the silica surfaces with PDDA, followed by centrifuging (8000 rpm, 3 min) and washing with DI water four times to remove excess PDDA. Afterward, the PDDA-coated silica spheres were dispersed in 100 mL of H<sub>2</sub>O again with a pH of 9 adjusted by diluted TBAOH solution and ultrasonically treated for another 5 min. A colloidal suspension of sonicated TBA<sub>1-x</sub>H<sub>x</sub>Ca<sub>2</sub>Nb<sub>3</sub>O<sub>10</sub> nanosheets (50 mL, concentration: 3 mg/mL) was added to the silica suspension dropwise under stirring. This procedure yielded flocculated sediment as a result of the electrostatic interaction of the nanosheets and silica spheres. The procedure lasted 1 h. After that, the solid was collected by centrifugation (4200 rpm, 4 min) and washed with dilute TBAOH solution (pH ~9) three times. The above

- (22) Sakai, N.; Fukuda, K.; Omomo, Y.; Ebina, Y.; Takada, K.; Sasaki, T. *J. Phys. Chem. C* **2008**, *112*(13), 5197–5202.
- (23) Maeda, K.; Eguchi, M.; Youngblood, W. J.; Mallouk, T. E. *Chem. Mater.* **2008**, *20*(21), 6770–6778.
- (24) Ida, S.; Ogata, C.; Eguchi, M.; Youngblood, W. J.; Mallouk, T. E.; Matsumoto, Y. *J. Am. Chem. Soc.* **2008**, *130*(22), 7052–7059.
- (25) Akatsuka, K.; Takanashi, G.; Ebina, Y.; Sakai, N.; Haga, M.; Sasaki, T. *J. Phys. Chem. Solids* **2008**, *69*(5–6), 1288–1291.
- (26) Shibata, T.; Sakai, N.; Fukuda, K.; Ebina, Y.; Sasaki, T. *Phys. Chem. Chem. Phys.* **2007**, *9*(19), 2413–2420.
- (27) Miyamoto, N.; Yamada, Y.; Koizumi, S.; Nakato, T. *Angew. Chem., Int. Ed. Engl.* **2007**, *46*(22), 4123–4127.
- (28) Akatsuka, K.; Ebina, Y.; Muramatsu, M.; Sato, T.; Hester, H.; Kumaresan, D.; Schmehl, R. H.; Sasaki, T.; Haga, M. A. *Langmuir* **2007**, *23*(12), 6730–6736.
- (29) Zhou, Y.; Ma, R. Z.; Ebina, Y.; Takada, K.; Sasaki, T. *Chem. Mater.* **2006**, *18*(5), 1235–1239.
- (30) Suzuki, S.; Miyayama, M. *J. Phys. Chem. B* **2006**, *110*(10), 4731–4734.
- (31) Izawa, K.; Yamada, T.; Unal, U.; Ida, S.; Altuntasoglu, O.; Koizumi, M.; Matsumoto, Y. *J. Phys. Chem. B* **2006**, *110*(10), 4645–4650.
- (32) Ida, S.; Unal, U.; Izawa, K.; Altuntasoglu, O.; Ogata, C.; Inoue, T.; Shimogawa, K.; Matsumoto, Y. *J. Phys. Chem. B* **2006**, *110*(47), 23881–23887.
- (33) Matsumoto, Y.; Unal, U.; Kimura, Y.; Ohashi, S.; Izawa, K. *J. Phys. Chem. B* **2005**, *109*(26), 12748–12754.
- (34) Sakai, N.; Ebina, Y.; Takada, K.; Sasaki, T. *J. Am. Chem. Soc.* **2004**, *126*(18), 5851–5858.
- (35) Kaschak, D. M.; Lean, J. T.; Waraksa, C. C.; Saupe, G. B.; Usami, H.; Mallouk, T. E. *J. Am. Chem. Soc.* **1999**, *121*(14), 3435–3445.
- (36) Keller, S. W.; Johnson, S. A.; Brigham, E. S.; Yonemoto, E. H.; Mallouk, T. E. *J. Am. Chem. Soc.* **1995**, *117*(51), 12879–12880.
- (37) Saupe, G. B.; Mallouk, T. E.; Kim, W.; Schmehl, R. H. *J. Phys. Chem. B* **1997**, *101*(14), 2508–2513.
- (38) Hoertz, P. G.; Mallouk, T. E. *Inorg. Chem.* **2005**, *44*(20), 6828–6840.
- (39) Hoffmann, M. R.; Martin, S. T.; Choi, W. Y.; Bahnemann, D. W. *Chem. Rev.* **1995**, *95*(1), 69–96.
- (40) Kamat, P. V.; Meisel, D. *Compt. Rend. Chim.* **2003**, *6*(8–10), 999–1007.

- (41) Stober, W.; Fink, A.; Bohn, E. *J. Colloid Interface Sci.* **1968**, *26*(1), 62–65.
- (42) Osterloh, F.; Hiramoto, H.; Porter, R.; Guo, T. *Langmuir* **2004**, *20*(13), 5553–5558.
- (43) Jacobsen, A. J.; Johnson, J. W.; Lewandowski, J. T. *Inorg. Chem.* **1985**, *24*, 3727–3729.
- (44) Schaak, R. E.; Mallouk, T. E. *Chem. Mater.* **2000**, *12*(9), 2513–2516.

**Table 1. Catalytic Activity Data; A = (TBA,H)Ca<sub>2</sub>Nb<sub>3</sub>O<sub>10</sub>, B = PA<sub>2</sub>K<sub>2</sub>Nb<sub>6</sub>O<sub>17</sub>**

	catalysts (masses of catalyst/nanosheets)							
	SiO <sub>2</sub> -A-A (1.5 g/51 mg)	SiO <sub>2</sub> -B-B (1.5 g/59 mg)	SiO <sub>2</sub> -A-B (1.5 g/56 mg)	SiO <sub>2</sub> -B-A (1.5 g/52 mg)	SiO <sub>2</sub> -A (3.0 g/51 mg)	SiO <sub>2</sub> -B (3.0 g/59 mg)	A (50 mg)	B (50 mg)
	20% MeOH							
pH before (after) irradiation	9.11 (8.61)	9.38 (8.78)	9.18 (8.51)	8.75 (7.89)	9.01 (8.42)	8.97 (8.29)	10.29	10.32
measured H <sub>2</sub> amount (μmol) after 5 h	80.1	146.0	363.5	196.4	62.7	191.1	107.2	458.3
calculated H <sub>2</sub> rate (μmol/h) per gram of nanosheet mass	314.2	495.0	1298	755.5	246.0 <sup>a</sup>	647.9 <sup>b</sup>	428.7	1833
	Pt-Loaded Samples in 20% MeOH							
pH before irradiation	8.64	8.92	8.72	8.92	8.92	8.67	8.95 <sup>c</sup>	8.70
measured H <sub>2</sub> amount (μmol) after 5 h	3126	4470	5337	4890	3086	5114	7803 <sup>c</sup>	3062
calculated H <sub>2</sub> rate (μmol/h) per gram of nanosheet mass	12257	15152	19061	18807	12100 <sup>a</sup>	17336 <sup>b</sup>	31212 <sup>c</sup>	12248

<sup>a</sup> Partial loss of nanosheets during centrifugation/washing. H<sub>2</sub> rate was adjusted to catalyst mass of SiO<sub>2</sub>-A-A. <sup>b</sup> Partial loss of nanosheets during centrifugation/washing. H<sub>2</sub> rate was adjusted to catalyst mass of SiO<sub>2</sub>-B-B. <sup>c</sup> 2 wt % Pt.

procedure was repeated to obtain double layers. For assembly of PA<sub>2</sub>K<sub>2</sub>Nb<sub>6</sub>O<sub>17</sub> nanosheets, diluted propylamine solution was used to adjust the pH of the solution.

**Heterostacked Assemblies.** Heterostacks composed of PDDA, TBA<sub>1-x</sub>H<sub>x</sub>Ca<sub>2</sub>Nb<sub>3</sub>O<sub>10</sub> and PA<sub>2</sub>K<sub>2</sub>Nb<sub>6</sub>O<sub>17</sub> nanosheets were formed by taking the SiO<sub>2</sub>/(PDDA/TBA<sub>1-x</sub>H<sub>x</sub>Ca<sub>2</sub>Nb<sub>3</sub>O<sub>10</sub>)<sub>n</sub> (*n* = 1) material from above and by dispersing it in 150 mL of PDDA solution with a pH of 9 adjusted with diluted propylamine solution. The suspension was then stirred for 20 min, followed by centrifuging (8000 rpm, 3 min) and washing with diluted propylamine solution (pH ~9) four times. The solid was dispersed in 100 mL of H<sub>2</sub>O with a pH of 9 adjusted by diluted propylamine solution and then added to a colloidal suspension of sonicated PA<sub>2</sub>K<sub>2</sub>Nb<sub>6</sub>O<sub>17</sub> nanosheets (50 mL, concentration 3 mg/mL) dropwise under stirring over the course of 1 h. The product was recovered by washing with diluted propylamine solution (pH ~9) and centrifuging (4200 rpm, 4 min) three times. Niobate nanosheets were used in excess to ensure complete coverage of the entire particle surface.

**Pt-Loaded Nanosheets.** Platinum nanoparticles were grown on the surfaces of nanosheets (both core-shell structures and pure nanosheets) by irradiating nanosheet materials in 20 vol% aqueous methanol containing 5 wt % (based on nanosheets) H<sub>2</sub>PtCl<sub>6</sub>·6H<sub>2</sub>O.<sup>16</sup> The reaction mixture was stirred in an Ar atmosphere and irradiated for 1 h. The product was collected by centrifugation (13 500 rpm, 10 min), washed twice with 50 mL aliquots of water, and stored in 25 mL of water for future studies.

**HF Etching for Nanosheet Mass Determination.** The core-shell composites were dissolved in 10% hydrofluoric acid solution. After 30 min the solids were separated by centrifugation and washed five times with deionized water. The as-obtained products were then dried in an oven at 80 °C for gravimetric analysis. The measured nanosheet masses are listed in Table 1.

**Photocatalytic H<sub>2</sub> Evolution Experiments.** Irradiation was performed at 30 °C using a Xe arc lamp with a measured irradiance of 400 mW/cm<sup>2</sup> at the glass flask surface. The photon flux over the spectral range of 250–500 nm was measured in the flask by ferrioxalate actinometry as 3.71238 × 10<sup>-6</sup> mol/s.<sup>45</sup> Photocatalytic H<sub>2</sub> evolution tests were performed by dispersing catalysts (refer to Table 1) in 50 mL aqueous methanol solution (MeOH, 20 vol %). Before measurements, UV light was illuminated onto the samples for 1 h to decompose the interlayer PDDA.

Then the flask was evacuated and purged four times with argon gas, and the stirred mixture was then irradiated for 5 h. Gas samples were periodically analyzed with a Varian gas chromatograph employing a Supelco molecular 60/80 sieve 5A column with Ar as the carrier gas and a thermal conductivity detector (TCD).

**Characterization.** Scanning electron microscopy (SEM) observations were performed with a JEOL JSM-5800LV instrument operated at 5 kV. SEM samples were sputter-coated with gold for observation. Transmission electron microscope (TEM) observations were conducted using a Philips CM120 instrument. UV/vis spectra were collected using an Ocean Optics HR2000 CG-UVNIR with a DH2000 light source. Infrared spectra were collected with a Galaxy Series FT-IR spectrophotometer from Mattson.

## Results and Discussion

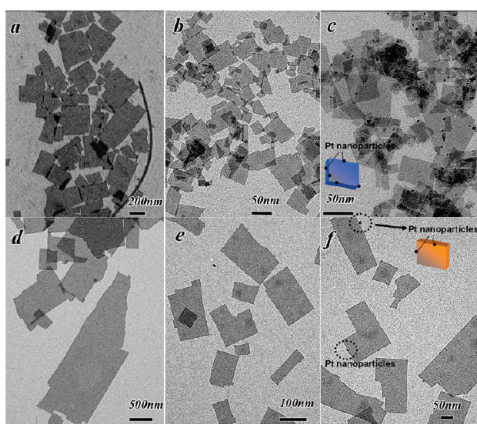
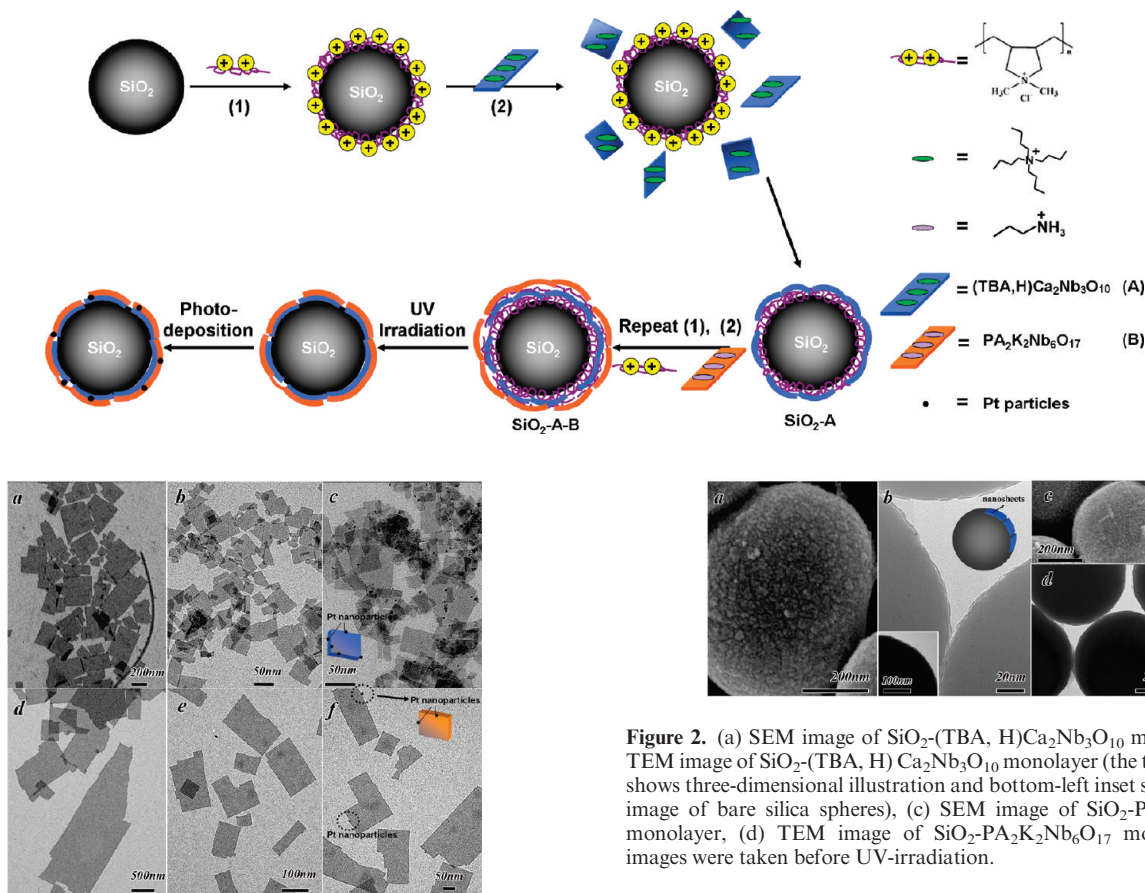
Scheme 1 shows the overall procedure for the layer-by-layer assembly of nanosheets and the removal of PDDA (poly(diallyldimethylammonium)) via UV irradiation. Take the formation of silica-(TBA, H)Ca<sub>2</sub>Nb<sub>3</sub>O<sub>10</sub>-PA<sub>2</sub>K<sub>2</sub>Nb<sub>6</sub>O<sub>17</sub> heterostacks as a typical example, in the first step, the surfaces of silica spheres were modified with PDDA chloride to be positively charged. Next, the negatively charged TBAOH exfoliated nanosheets were adsorbed onto the surfaces of PDDA modified spheres to form core-shell composites because of the electrostatic attraction between them. Step 1 was then repeated to modify the negatively charged monolayer surfaces with PDDA again. Finally, the negatively charged PA exfoliated nanosheets were adsorbed onto the modified surfaces to form silica-(TBA, H)Ca<sub>2</sub>Nb<sub>3</sub>O<sub>10</sub>-PA<sub>2</sub>K<sub>2</sub>Nb<sub>6</sub>O<sub>17</sub> heterostacked double-layer spheres.

The procedures for other monolayer and double-layer samples are similar (details are described in the Experimental Section). The resulting core-shell composites were then irradiated with light from a 300 W Xe arc lamp to photochemically convert the PDDA into NH<sub>4</sub><sup>+</sup> and other oxidation products.<sup>46,47</sup> FTIR measurements were

(45) Kuhn, H. J.; Braslavsky, S. E.; Schmidt, R. *Pure Appl. Chem.* **2004**, *76*(12), 2105–2146.

(46) Wang, L.; Sasaki, T.; Ebina, Y.; Kurashima, K.; Watanabe, M. *Chem. Mater.* **2002**, *14*(11), 4827–4832.

(47) Yanagida, S.; Nakajima, A.; Sasaki, T.; Kameshima, Y.; Okada, K. *Chem. Mater.* **2008**, *20*(11), 3757–3764.

**Scheme 1. Schematic Illustration of the Overall Procedures for the Layer-by-Layer Assembly of Nanosheets to Form SiO<sub>2</sub> Homo- and Heterostacks**


**Figure 1.** TEM images of (a) (TBA, H)Ca<sub>2</sub>Nb<sub>3</sub>O<sub>10</sub> nanosheets before sonication, (b) (TBA, H)Ca<sub>2</sub>Nb<sub>3</sub>O<sub>10</sub> nanosheets after 50 min of sonication, (c) Pt-loaded sonicated (TBA, H)Ca<sub>2</sub>Nb<sub>3</sub>O<sub>10</sub> nanosheets, (d) PA<sub>2</sub>K<sub>2</sub>Nb<sub>6</sub>O<sub>17</sub> nanosheets before sonication, (e) PA<sub>2</sub>K<sub>2</sub>Nb<sub>6</sub>O<sub>17</sub> nanosheets after 2 h of sonication, (f) Pt-loaded sonicated PA<sub>2</sub>K<sub>2</sub>Nb<sub>6</sub>O<sub>17</sub> nanosheets.

employed to monitor this process. However, the content of PDDA in silica/PDDA/nanosheets composites was below the IR detection limit (see Figure S1 in the Supporting Information). Platinum nanoparticles were grown on the surfaces of nanosheets by photodeposition in the presence of methanol, using H<sub>2</sub>PtCl<sub>6</sub> as precursor.

Edge lengths of unsonicated (TBA, H)Ca<sub>2</sub>Nb<sub>3</sub>O<sub>10</sub> and PA<sub>2</sub>K<sub>2</sub>Nb<sub>6</sub>O<sub>17</sub> nanosheets range from 200 to 500 nm (Figure 1a) and 500 to 1500 nm (Figure 1d), respectively. The lateral size of nanosheets depends on the crystal size of the starting materials and the mechanical stress during the delamination process. The sizes are about the same as the diameter of silica spheres (450 nm), so it would be difficult to achieve good adhesion, because of the curvature of the spheres. Sonication procedures were used to obtain smaller nanosheets for better absorption and higher coverage. After sonication, the two-dimensional sizes of the nanosheets decreased significantly, to about 20 to 50 nm for (TBA, H)Ca<sub>2</sub>Nb<sub>3</sub>O<sub>10</sub> nanosheets (Figure 1b) and to 100 to 200 nm for PA<sub>2</sub>K<sub>2</sub>Nb<sub>6</sub>O<sub>17</sub> nanosheets (Figure 1e). Platinum nanoparticles were photochemically deposited onto individual nanosheets, as described

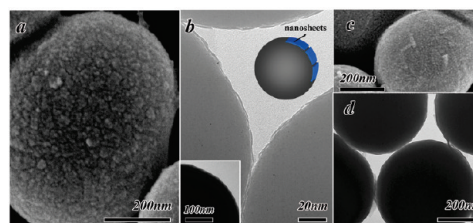


**Figure 2.** (a) SEM image of SiO<sub>2</sub>-(TBA, H)Ca<sub>2</sub>Nb<sub>3</sub>O<sub>10</sub> monolayer, (b) TEM image of SiO<sub>2</sub>-(TBA, H)Ca<sub>2</sub>Nb<sub>3</sub>O<sub>10</sub> monolayer (the top right inset shows three-dimensional illustration and bottom-left inset shows a TEM image of bare silica spheres), (c) SEM image of SiO<sub>2</sub>-PA<sub>2</sub>K<sub>2</sub>Nb<sub>6</sub>O<sub>17</sub> monolayer, (d) TEM image of SiO<sub>2</sub>-PA<sub>2</sub>K<sub>2</sub>Nb<sub>6</sub>O<sub>17</sub> monolayer. All images were taken before UV-irradiation.

above. TEM images reveal that Pt nanoparticles deposited mainly along the edges of the nanosheets (Figure 1e,f).

The formation of core–shell structures is observed by SEM and TEM. Figure 2a shows the SEM image of SiO<sub>2</sub>-(TBA, H)Ca<sub>2</sub>Nb<sub>3</sub>O<sub>10</sub> monolayer sphere. A noticeable difference for the spheres with or without nanosheets is the surface roughness. The edges of the nanosheets on the surfaces can be clearly identified. The sizes of nanosheets are estimated to be 20–50 nm, which coincide with TEM results in Figure 1b. The surface details are further observed by TEM (Figure 2b). Comparing to bare silica spheres (inset of Figure 2b and Figure S2a in the Supporting Information) and SiO<sub>2</sub>/PDDA spheres (Figure S2b in the Supporting Information), the thin nanosheet layer on the SiO<sub>2</sub> surface becomes apparent. It has been reported that the thickness of (TBA, H)Ca<sub>2</sub>Nb<sub>3</sub>O<sub>10</sub> sheets is 1.16 nm, which agrees with the TEMs in Figures 2–4.<sup>7</sup> The micrographs also indicate that the surface coverage for (TBA, H)Ca<sub>2</sub>Nb<sub>3</sub>O<sub>10</sub> nanosheets is very high, at least 80–90% by rough estimation. Meanwhile, no double layers are observed, likely because of repulsion between negatively charged nanosheets.

Similarly, SEM images of SiO<sub>2</sub>-PA<sub>2</sub>K<sub>2</sub>Nb<sub>6</sub>O<sub>17</sub> monolayer (Figure 2c) show that the PA<sub>2</sub>K<sub>2</sub>Nb<sub>6</sub>O<sub>17</sub> nanosheets successfully assemble onto the surfaces of silica spheres. Since the sizes of sonicated PA<sub>2</sub>K<sub>2</sub>Nb<sub>6</sub>O<sub>17</sub> nanosheets are larger, the surface morphologies of the core–shell composites are different. There are some nanoparticles discernible on the surfaces. These are likely gold nanoparticles formed

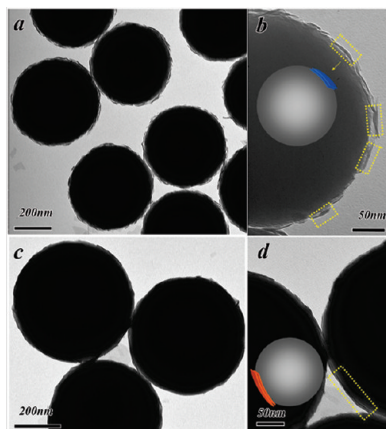


**Figure 3.** TEM images of (a)  $\text{SiO}_2$ -(TBA, H) $\text{Ca}_2\text{Nb}_3\text{O}_{10}$  homostacked double-layer, (b) magnified image of  $\text{SiO}_2$ -(TBA, H) $\text{Ca}_2\text{Nb}_3\text{O}_{10}$  double layer (inset shows a 3D illustration), (c)  $\text{SiO}_2$ - $\text{PA}_2\text{K}_2\text{Nb}_6\text{O}_{17}$  homostacked double layer, (d) magnified image of  $\text{SiO}_2$ - $\text{PA}_2\text{K}_2\text{Nb}_6\text{O}_{17}$  double layer (inset shows 3D illustration). All images were taken before UV-irradiation.

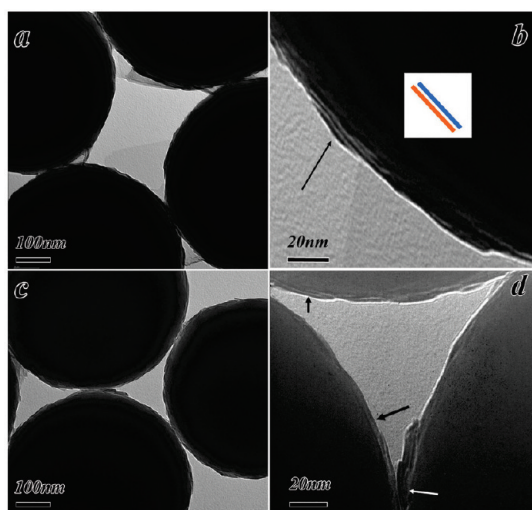


**Figure 4.** TEM images of (a)  $\text{SiO}_2$ -(TBA, H) $\text{Ca}_2\text{Nb}_3\text{O}_{10}$ - $\text{PA}_2\text{K}_2\text{Nb}_6\text{O}_{17}$  heterostacks, (b) magnified image of  $\text{SiO}_2$ -(TBA, H) $\text{Ca}_2\text{Nb}_3\text{O}_{10}$ - $\text{PA}_2\text{K}_2\text{Nb}_6\text{O}_{17}$  heterostacks (the inset shows a 2D illustration), (c)  $\text{SiO}_2$ - $\text{PA}_2\text{K}_2\text{Nb}_6\text{O}_{17}$ -(TBA, H) $\text{Ca}_2\text{Nb}_3\text{O}_{10}$  heterostacks, (d) magnified image of  $\text{SiO}_2$ - $\text{PA}_2\text{K}_2\text{Nb}_6\text{O}_{17}$ -(TBA, H) $\text{Ca}_2\text{Nb}_3\text{O}_{10}$  heterostacks. All images were taken before UV-irradiation.

during gold sputtering before SEM observation. The TEM image (Figure 2d) further demonstrates the adsorption of  $\text{PA}_2\text{K}_2\text{Nb}_6\text{O}_{17}$  nanosheets onto silica surfaces.

Figure 3 shows TEM images of homostacked double-layers of the two niobates. The surfaces of double-layer products (Figure 3a,c and Figure S3 in the Supporting Information) are much rougher than monolayer ones. As the niobate nanosheet is very thin compared with the diameter of silica spheres, almost no apparent increase in the particle diameter is seen. Magnified images reveal the homostacking as shown in Figure 3b,d. The intersheet distances are estimated to be 1–3 nm. Figure 4 shows typical TEM images of heterostacked double layers. The presence of stacks can be clearly seen in the images. The stacking distance of 1–3 nm is similar to that of the homostacks.

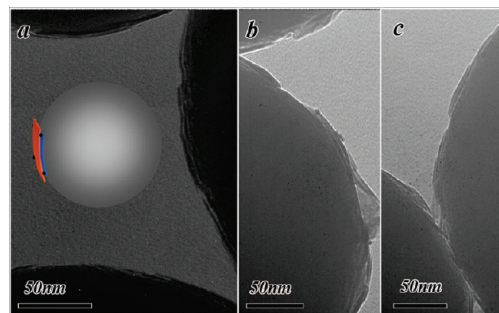


**Figure 5.** TEM images of (a)  $\text{Pt}/\text{SiO}_2$ -(TBA, H) $\text{Ca}_2\text{Nb}_3\text{O}_{10}$  double layer (the inset shows a 3D illustration), (b)  $\text{Pt}/\text{SiO}_2$ -(TBA, H) $\text{Ca}_2\text{Nb}_3\text{O}_{10}$ - $\text{PA}_2\text{K}_2\text{Nb}_6\text{O}_{17}$  heterostacks, (c)  $\text{Pt}/\text{SiO}_2$ - $\text{PA}_2\text{K}_2\text{Nb}_6\text{O}_{17}$ -(TBA, H) $\text{Ca}_2\text{Nb}_3\text{O}_{10}$  heterostacks.

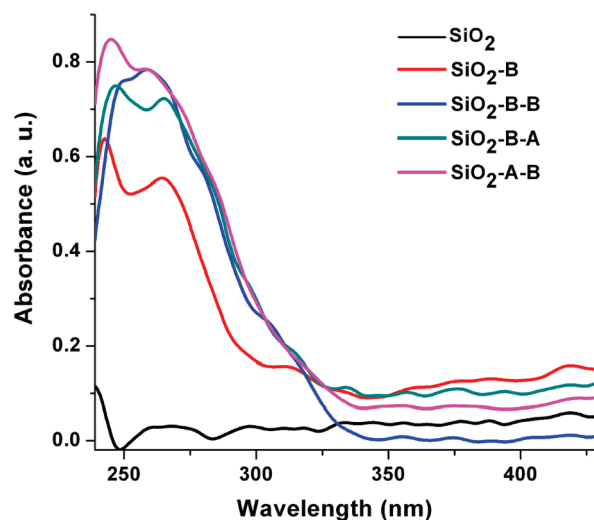


**Figure 6.** Diffuse reflectance UV-visible spectra of bare silica spheres and core-shell composites. A = (TBA, H) $\text{Ca}_2\text{Nb}_3\text{O}_{10}$ , B =  $\text{PA}_2\text{K}_2\text{Nb}_6\text{O}_{17}$ .

Figure 5 shows typical TEM images of Pt-loaded double-layer composites. The images demonstrate that the stacks can survive 7 h of irradiation in 20 vol % methanol aqueous solution without significant change. Platinum nanoparticles are difficult to detect in these images, probably due to the low mass percentage. As mentioned above, Pt nanoparticles prefer to deposit along the edges of the nanosheets, thus they are not easy to observe as illustrated by the 3D illustration in the inset of Figure 5a. However, the Pt-loaded silica-based composites turned out to be brown in color (see Figure S4 in the Supporting Information), indicative of the presence of Pt nanoparticles.

Figure 6 shows diffuse reflectance UV-visible spectra of bare silica spheres and core-shell composites. Bare silica spheres show no absorption band around 250–400 nm. The nanosheet semiconductors are known to absorb light in the ultraviolet region of the spectrum with an absorption edge at around 350 nm.<sup>6,7</sup> The spectra for the core-shell monolayer composites clearly reproduce the optical characteristics of the niobate nanosheets. The absorbance at 250–350 nm becomes stronger in the double-layer compounds, confirming the successful LBL assembly of niobate nanosheets on silica spheres. The

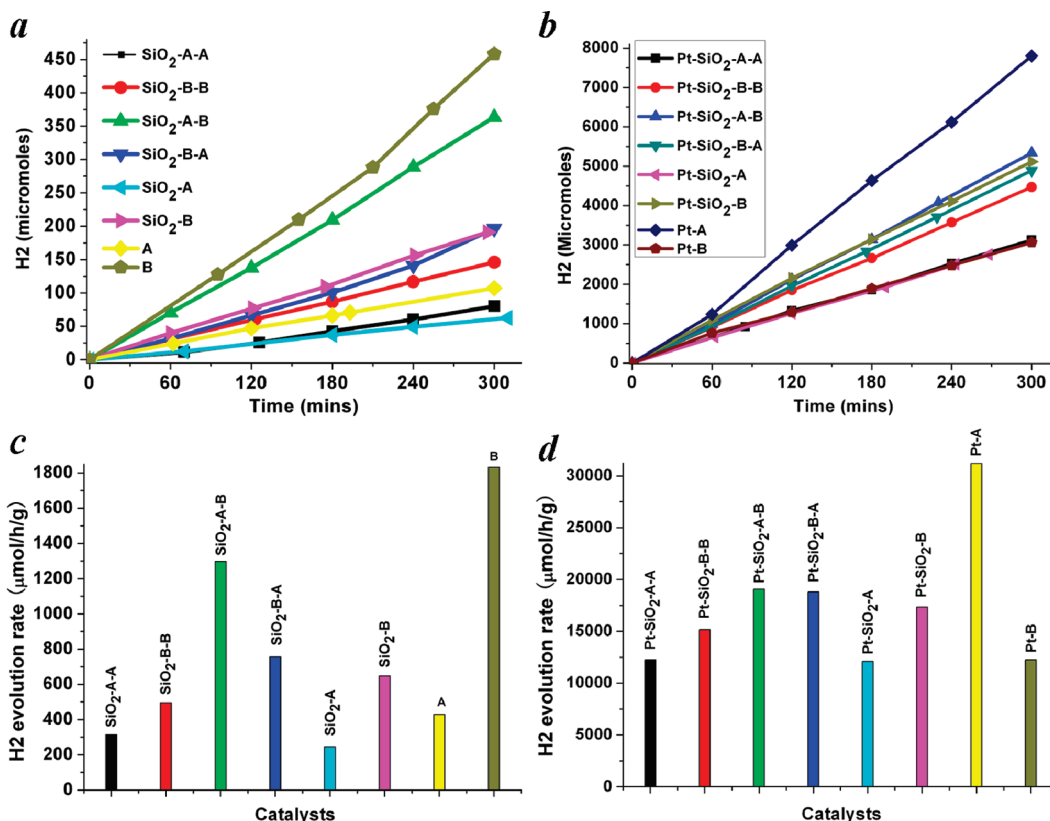


**Figure 7.** (a) Experimental H<sub>2</sub> evolution from core-shell structures in 20 vol % aqueous methanol. (b) Experimental H<sub>2</sub> evolution of Pt-loaded samples in 20 vol % aqueous methanol. (c) Calculated H<sub>2</sub> evolution rates from panel a per gram of nanosheet mass. (d) calculated H<sub>2</sub> evolution rates from panel b per gram of nanosheet mass. A = (TBA,H) Ca<sub>2</sub>Nb<sub>3</sub>O<sub>10</sub>, B = PA<sub>2</sub>K<sub>2</sub>Nb<sub>6</sub>O<sub>17</sub>.

optical data are consistent with the structural characterizations by SEM and TEM as described above.

Photocatalytic studies of all materials were carried out as described in the Experimental Section. Time-resolved data for H<sub>2</sub> evolution from 20% aqueous methanol is presented in Figure 7, whereas numerical data is given in Table 1. To ensure equal amounts of active catalyst in each test, 3.0 g of the single-layer coated SiO<sub>2</sub> spheres were used and 1.5 g of double layer coated ones. Considering the specific surface area of SiO<sub>2</sub> spheres and the densities of the nanosheet layers, each sample was estimated to contain 50–60 mg nanosheets, assuming 100% coverage. Exact amounts were measured with gravimetric analysis, after dissolving SiO<sub>2</sub> spheres with diluted HF solution. Nanosheet masses thus obtained are listed in the first row of Table 1.

After an initial irradiation to decompose adsorbed PDDA and PA, all core-shell structures samples evolve H<sub>2</sub> linearly (Figure 7a), producing between 62.7 and 364 μmol of H<sub>2</sub> after 5 h. Interestingly, SiO<sub>2</sub>-PDDA by itself also evolved some H<sub>2</sub> (see Figure S5 in the Supporting Information), but the overall amount of 6.9 μmol after 5 h was negligible in comparison with the core-shell structures.

To compare activities among core-shell structures, we employ H<sub>2</sub> rates [μmol/h/g] in Figure 7c that are based on the measured nanosheet mass. It can be seen that the activity of the heterostacks SiO<sub>2</sub>-A-B and SiO<sub>2</sub>-B-A is about 2–4 times of the homostacks SiO<sub>2</sub>-A-A and

SiO<sub>2</sub>-B-B on average. The activity of the heterostacks also depends on the stacking order. It is high when PA<sub>2</sub>K<sub>2</sub>Nb<sub>6</sub>O<sub>17</sub> sheets are on top (SiO<sub>2</sub>-A-B) and low when they are at the bottom (SiO<sub>2</sub>-B-A), near the SiO<sub>2</sub> substrate. The enhanced catalytic activity and its dependence on the stacking sequence are indications of a nanosheet heterojunction. Such a junction would enable photochemical charge separation among the two nanosheets, prolong electron/hole lifetimes, and promote reactions with water and methanol.<sup>48</sup> However, further studies are required to confirm this hypothesis.

The data in Figure 7c reveals no significant differences between monolayer and double-layer samples (SiO<sub>2</sub>-A-A, SiO<sub>2</sub>-B-B, SiO<sub>2</sub>-A, SiO<sub>2</sub>-B), after correcting for differences in nanosheet mass. The fact that nanosheets in direct contact with the SiO<sub>2</sub> substrate perform equally to nanosheets away from SiO<sub>2</sub> shows that the activity of the nanosheets is not affected by the SiO<sub>2</sub> substrate and the anchoring groups.

Comparing the SiO<sub>2</sub> supported nanosheets with freely dispersed nanosheet samples (A and B), one can see that the catalytic activity in the SiO<sub>2</sub> samples is diminished. Based on the performance of the double stacks, direct chemical interactions with the SiO<sub>2</sub> can be ruled out as cause for the diminished activity. A more probable reason

(48) Uchida, S.; Yamamoto, Y.; Fujishiro, Y.; Watanabe, A.; Ito, O.; Sato, T. *J. Chem. Soc., Faraday Trans.* **1997**, 93(17), 3229–3234.

(49) Hitoki, G.; Takata, T.; Kondo, J. N.; Hara, M.; Kobayashi, H.; Domen, K. *Chem. Commun.* **2002**, No. 16, 1698–1699.

is the strong light scattering caused by the large amounts of silica spheres, which interferes with light-harvesting of the nanosheets. Among the nonsupported nanosheets,  $\text{PA}_2\text{K}_2\text{Nb}_6\text{O}_{17}$  nanosheets (B) show the highest activity for  $\text{H}_2$  evolution, which is two times above (TBA,H)- $\text{Ca}_2\text{Nb}_3\text{O}_{10}$  (A). We attribute this to the presence of surface-adsorbed PA, which can act a sacrificial electron donor.<sup>6</sup> Tetrabutylammonium (TBA) ion, on the other hand, does not under these conditions.

In general, the function of water splitting photocatalysts is known to be limited by high electrochemical overpotentials for the hydrogen evolution reaction (HER) on metal oxide surfaces.<sup>2</sup> To reduce this limitation, core-shell structures were modified with 5% mass Pt (based on nanosheets) using photochemical deposition. The data in Figure 7b shows that Pt does indeed enhance the activity of the catalysts significantly. After correcting for differences in catalyst mass (Figure 7d) the Pt-modified heterostack samples  $\text{SiO}_2$ -A-B and  $\text{SiO}_2$ -B-A are most active, with the former evolving  $\text{H}_2$  at a rate of 19 mmol/h/g at pH 8.72, which is  $\sim 14$  times higher than the Pt-free heterostack. The remaining samples maintain the same relative order of activity as in Figure 7c, although the absolute differences between samples are reduced. The activity of nonsupported platinum-loaded nanosheets is comparable or higher to the core-shell structures, with Pt-(TBA, H) $\text{Ca}_2\text{Nb}_3\text{O}_{10}$  now being the most active catalyst at 31.2 mmol/h/g. Again, we attribute this higher activity to increased light penetration through the sample (reduced scattering due to absence of  $\text{SiO}_2$ ).

## Conclusion

In conclusion, we have presented a layer-by-layer assembly approach for the generation of inorganic core-shell structures that are active for photocatalytic  $\text{H}_2$  evolution in the presence of methanol as sacrificial donor. Ultrasonicated (TBA, H) $\text{Ca}_2\text{Nb}_3\text{O}_{10}$  and  $\text{PA}_2\text{K}_2\text{Nb}_6\text{O}_{17}$  nanosheets were used as the building blocks for the construction of the catalysts. The lateral nanosheet distribution on the  $\text{SiO}_2$  spheres could be directly observed with SEM while the stacking could be directly observed with TEM. For  $\text{H}_2$  evolution, core-shell structures were only slightly less active than the freely dispersed nanosheets, which we attribute to reduced light penetration due to the strongly scattering  $\text{SiO}_2$  spheres. A-B stacks were more active than A-A and B-B stacks, the latter being comparable to single layers A and B (at equal mass). Upon Pt loading the activity differences between homostacked and heterostacked samples became less pronounced. PDDA-coated  $\text{SiO}_2$  spheres showed only negligible activity for photochemical hydrogen evolution from aqueous methanol.

**Acknowledgment.** This project was supported by the National Science Foundation (Grant 0829142). H. Zhou is grateful for receiving support from the Chinese study abroad fund.

**Supporting Information Available:** IR spectra and SEM images of  $\text{SiO}_2$ /PDDA/nanosheet composites and TEM images of bare and PDDA-coated silica spheres; photo of the Pt-loaded  $\text{SiO}_2$  nanosheet composites, and photochemical  $\text{H}_2$  evolution data from PDDA-coated silica spheres (PDF). This material is available free of charge via the Internet at <http://pubs.acs.org/>.